



OPEN ACCESS

EDITED BY
Rosaria Anna Picca,
University of Bari Aldo Moro, Italy

REVIEWED BY
Jiahao Huang,
Affiliated Hospital of Guangdong
Medical University, China
Seyed Hadi Badri,
Islamic Azad university, Iran

*CORRESPONDENCE
Jessica Z. Kubicek-Sutherland,
jzk@lanl.gov

SPECIALTY SECTION
This article was submitted to
Biosensors,
a section of the journal
Frontiers in Sensors

RECEIVED 19 May 2022
ACCEPTED 16 September 2022
PUBLISHED 04 October 2022

CITATION
Kocheril PA, Lenz KD, Jacobsen DE and
Kubicek-Sutherland JZ (2022),
Amplification-free nucleic acid
detection with a fluorescence-based
waveguide biosensor.
Front. Sens. 3:948466.
doi: 10.3389/fsens.2022.948466

COPYRIGHT
© 2022 Kocheril, Lenz, Jacobsen and
Kubicek-Sutherland. This is an open-
access article distributed under the
terms of the [Creative Commons
Attribution License \(CC BY\)](https://creativecommons.org/licenses/by/4.0/). The use,
distribution or reproduction in other
forums is permitted, provided the
original author(s) and the copyright
owner(s) are credited and that the
original publication in this journal is
cited, in accordance with accepted
academic practice. No use, distribution
or reproduction is permitted which does
not comply with these terms.

Amplification-free nucleic acid detection with a fluorescence-based waveguide biosensor

Philip A. Kocheril, Kiersten D. Lenz, Daniel E. Jacobsen and
Jessica Z. Kubicek-Sutherland*

Physical Chemistry and Applied Spectroscopy, Chemistry Division, Los Alamos National Laboratory, Los Alamos, NM, United States

Early detection of pathogens using nucleic acids in clinical samples often requires sensitivity at the single-copy level, which currently necessitates time-consuming and expensive nucleic acid amplification. Here, we describe 1) a redesigned flow cell in the shape of a trapezoid-subtracted geometric stadium, and 2) modified experimental procedures that allow for the measurement of sub-attomolar analytes in microliter quantities on a fluorescence-based waveguide biosensor. We verified our instrumental sensitivity with a 200- μ L sample of a fluorescent streptavidin conjugate at 100 zM (100 zeptomolar, or $100 \cdot 10^{-21}$ mol L⁻¹) and theoretically explored the applicability of this modified sensing platform in a sandwich immunoassay format using a Langmuir adsorption model. We present assays that demonstrate specific detection of synthetic influenza A DNA (in buffer) and RNA (in saliva) oligonucleotides at the single-copy level (200 μ L at 10 zM) using a fluorescent molecular beacon. Lastly, we demonstrate detection of isolated genomic influenza A RNA at a clinically relevant concentration. This work constitutes a sensitivity improvement of over twelve orders of magnitude compared to our previous nucleic acid detection work, illustrating the significant enhancements that can be gained with optimized experimental design.

KEYWORDS

waveguide, fluorescence spectroscopy, nucleic acid, amplification-free, molecular beacon, langmuir adsorption, single molecule

1 Introduction

The limit of detection of a sensor defines the minimum amount or concentration of an analyte of interest at which signal can be confidently discerned from noise (Long and Winefordner, 1983). Limits of detection are important quantities for biosensors, as they play a role in determining the scope of measurable targets for the sensor in biofluid samples (Kelley, 2017).

The ultimate limit of detection of any sensor is a single analyte molecule (Li et al., 2020). The first report of optical single-molecule detection by Moerner and Kador (1989) used frequency-modulation spectroscopy with Stark or ultrasonic modulation to remove background interference. Shortly thereafter, Orrit and Bernard (1990) reported single-molecule detection with fluorimetry, a method that quickly became popular for single-molecule detection due in part to its minimal background signal (Orrit and Bernard, 1990). Over the past few decades, single-molecule analytical techniques have developed significantly, allowing for deep insights into excited state lifetimes, dynamics in complex systems, and more (Moerner and Fromm, 2003).

Biosensors capable of single-molecule detection are of significant interest, as they hold unmatched potential to characterize the early stages of disease and monitor treatment progress (Akkilic et al., 2020). Single-molecule biosensing requires not only the instrumental sensitivity to measure signal from single analytes, but the analytical sensitivity of high-affinity biomolecular interactions, thoughtful assay design, and replicate measurements to account for the significant sampling variability that occurs in experiments at the single-molecule level (Battich et al., 2013; Zhang et al., 2014). Several single-molecule biosensors have been reported using a variety of sensing modalities, including electrochemical sensing, plasmonic sensing, interferometry, and fluorescence spectroscopy and microscopy (Huang et al., 2008; Zevenbergen et al., 2011; Baaske et al., 2014; Assad et al., 2017; Cohen and Walt, 2017; Landry et al., 2017; Mauranyapin et al., 2017; Fan et al., 2019; Akkilic et al., 2020).

It is worth noting that single-molecule sensitivity is not needed in many biosensing applications, as evidenced by the widespread usage of methods such as enzyme-linked immunosorbent assays and electrophoretic mobility shift assays (Wong et al., 2014; Zhang et al., 2014; Ma et al., 2021). As noted by Kelley (2017), most biological analytes have concentrations in the attomolar or above, and most biofluid samples can be readily obtained in milliliter quantities. However, single-molecule biosensing holds potential to reduce the amount of biofluid needed for diagnostic assays; furthermore, sensitivity at the single-copy level is valuable for respiratory viral diagnostics, given the low copy numbers of nucleic acids from respiratory viruses that can be observed in nasal samples (Lee et al., 2009; Courtney et al., 2021a).

Amplification-based methods, such as the polymerase chain reaction (PCR), currently dominate nucleic acid detection strategies for their sensitivity, broad applicability to different nucleic acid targets, and compatibility with a variety of sample types (Kumar and Henrickson, 2012; Courtney et al., 2021a). However, the assay time, sensitivity to contamination, and cost of the laboratory instrumentation and reagents required for PCR can be prohibitive to rapid and accessible diagnostics and biosurveillance, and some PCR assays have restricted

availability (Courtney et al., 2021a). Therefore, other technologies that are capable of directly detecting nucleic acids at the single-copy level are valuable and an active area of research (Nakane et al., 2004; Johnson-Buck et al., 2015; Du and Dong, 2017; Aman et al., 2020; Courtney et al., 2021a; Courtney et al., 2021b). For a comprehensive review of nucleic acid biosensing technologies, see Courtney et al., 2021a.

The patient samples used as clinical standards for the diagnosis of viruses like influenza are nasopharyngeal aspirates and nasopharyngeal swabs (To et al., 2019). However, the collection of these specimens causes discomfort to patients and presents significant risk to healthcare workers (Frazee et al., 2018). Other sample types—most notably, saliva—have been explored as safer and more convenient alternatives to the standard nasopharyngeal samples, but saliva tests generally exhibit lower sensitivity (To et al., 2019). Therefore, there is a significant need for sensitive nucleic acid biosensing platforms to achieve reliable biosensing in sample types like saliva.

Our laboratory and others have previously described the use of optical waveguides for sensitive and specific biosensing (Golden et al., 2005; Taitt et al., 2016; Liu et al., 2017a; Liu et al., 2017b; Chen and Wang, 2020; Kocheril et al., 2022). Among biosensing approaches, evanescent field-stimulated fluorimetry has the advantages of spatial specificity, sensitivity to low-concentration analytes, applicability to complex biofluid samples with minimal processing, and compatibility with fast, low-noise detectors (Benito-Pena et al., 2016). Evanescent fields do not extend far past the surface of a waveguide, so analytes must be held close to the surface, thereby concentrating them and yielding high sensitivity. Waveguide biosensing assays commonly rely on surface-anchored biomolecules that interact with detection targets. Surface coatings for these biosensing assays commonly include supported lipid bilayers, which can be made broadly compatible with a variety of biological substrates through the use of biotinylated lipids and bioconjugation of biotin or streptavidin (Attwood et al., 2013). Using a planar waveguide-based optical biosensor, our laboratory has previously reported detection of influenza RNA oligonucleotides with biotinylated DNA molecular beacons (MBs), which exhibit fluorescence upon hybridizing to a target nucleic acid sequence due to the physical separation of fluorophore and quencher moieties bound to opposite sides of the MB (Courtney et al., 2021b). However, the lowest RNA concentration reported with this sensor was 50 nM in buffer in a 100- μ L sample (an estimated three trillion copies of RNA), and we have not previously approached single-molecule detection with this biosensing platform.

Here, we detail the modified flow cell design and bilayer preparation procedures that provide a sensitivity enhancement of over twelve orders of magnitude to our biosensor platform (as compared to our previous measurements with RNA), allowing for detection of analytes at the single-molecule level. As

validation of our instrumental sensitivity, we measured fluorescence from 200 μL of a fluorescent streptavidin conjugate at 100 zM (100 zeptomolar, or $100 \cdot 10^{-21} \text{ mol L}^{-1}$)—an estimated twelve analyte molecules. To explore the applicability of our sensor in antibody (Ab) sandwich fluorescence assays, we used a Langmuir adsorption model; though initially developed to describe the adsorption of gases onto solid planar surfaces, this model is now broadly used to quantify the adsorption of molecules in solution as a function of their concentration (Langmuir, 2002; Sohn and Kim, 2005; Zhang et al., 2014). As an assessment of analytical sensitivity in a biologically relevant assay architecture, we demonstrate specific nucleic acid detection from 200 μL of an influenza A DNA (IAD) oligonucleotide at 10 zM—an estimated single copy of IAD—using an MB developed in the Fast Evaluation of Viral Emerging Risks (FEVER) pipeline (Courtney et al., 2021b; Stromberg et al., 2022). Lastly, we demonstrate detection of zM influenza A RNA (IAR) oligonucleotide and genomic IAR spiked into normal human saliva at a clinically relevant concentration using the same MB and explore the concentration dependence of our assays across multiple orders of magnitude.

2 Materials and methods

2.1 Biosensor instrumentation

The sensing components of our waveguide biosensor have been described previously (Grace et al., 2004). In brief, 532-nm light from a frequency-doubled diode-pumped laser (GCL-025-S, CrystaLaser LC, Reno, NV, United States; 25 mW) is passed through a one-stop neutral density filter, a polarizing filter, and a zero-order half-wave plate, attenuating the laser's total power to approximately 520 μW to minimize photobleaching during data acquisition and allow for more efficient coupling. The beam is passed through a mechanical shutter (Model 845 HP, Newport Corporation, Irvine, CA, United States) and focused ($f = 200 \text{ mm}$; beam waist approximately 1 mm) onto the diffraction grating of a 120-nm-thick silicon oxynitride single-mode planar optical waveguide (nGimat Ltd., Atlanta, GA, United States) coated with a 10-nm silicon dioxide film (Spectrum Thin Films Inc. Hauppauge, NY, United States), the design and fabrication of which has been described previously (Mukundan et al., 2009). The light that is not reflected or scattered off the surface of the waveguide (approximately 130 μW) or coupled into the silicon oxynitride thin film (approximately 300 μW) is transmitted through the flow cell and monitored with a silicon photodiode power meter (S116C, Thorlabs, Newton, NJ, United States). The light coupled into the thin film generates an evanescent field, which excites fluorophores held near the surface of the waveguide. Isotropically emitted fluorescence is collected with a fiber-

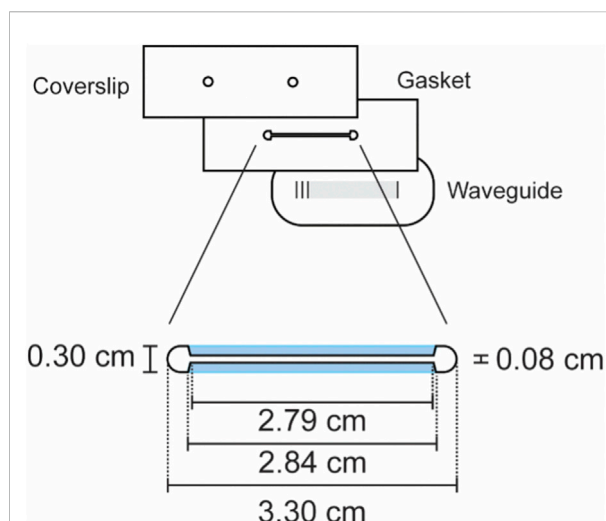


FIGURE 1

Trapezoid-subtracted geometric stadium flow cell design. The surface area of this 0.5-mm-thick flow cell is approximately 34.9 mm^2 , giving the cell a volume of approximately 17.4 μL . Blue regions denote the trapezoids that were subtracted from a geometric stadium to yield this particular geometry.

optic cable (QP600-025-UV-BX, Ocean Insight, Orlando, FL, United States; held roughly normal, 1 mm from the surface of the waveguide). The collected light is routed through a 532-nm long-pass filter and coupled into a fiber-optic spectrometer (P-600-2-UV-VIS, Ocean Insight; OceanOptics USB 2000, Ocean Insight). The resulting data is transmitted to a computer running a LabVIEW-based Virtual Instrument that coordinates the shutter control with data acquisition and processes spectra (SCB-68, National Instruments, Austin, TX, United States; LabVIEW v7.1, National Instruments; OmniDriver, Ocean Insight).

2.2 Flow cell preparation

A planar optical waveguide and a glass coverslip (microscope slide measuring 7.62 cm \times 2.54 cm with two 1-mm holes drilled 1.5 cm from the center along the long axis of the slide; 48300-036, VWR International, Radnor, PA, United States) were cleaned for 5 min each in chloroform (319,988, Millipore Sigma, St. Louis, MO, United States), ethanol (EX0276, Millipore Sigma), and ultrapure water (Direct-Q 3 UV-R, Millipore Sigma) by bath sonication (2510R-DTH Ultrasonic Cleaner, Branson Ultrasonics, Brookfield, CT, United States), dried under argon gas (Aircas, Radnor, PA, United States), and further cleaned by ultraviolet-ozone treatment (L2002A2-US, Ossila Ltd., Sheffield, UK; Model T10 \times 10/OES, UVOCS Inc. Lansdale, PA, United States) for 40 min. A 0.5-mm-thick hydrophobic gasket (CultureWell Silicone Sheet Material RD477403-M,

Grace Bio-Labs, Bend, OR, United States) was laser-cut to 7.62 cm × 2.54 cm with a cutout in the shape of a trapezoid-subtracted geometric stadium (TSGS; see [Figure 1](#) for dimensions). The cleaned waveguide and coverslip were bonded together with the TSGS silicone gasket to form an approximately 17.4-μL flow cell. The waveguide-gasket-coverslip assembly was screw-mounted between two pieces of a custom-milled housing fitted with an O-ring-sealed septum (inlet) and an O-ring-sealed drain tube (outlet) that align with the holes on the coverslip.

2.3 Lipid preparation

30 μL of 0.6 mM 1,2-dioleoyl-sn-glycero-3-phosphoethanolamine-*N*-(cap biotinyl) (DOPE-biotin; 870,273, Avanti Polar Lipids, Alabaster, AL, United States) in chloroform was deposited in a glass test tube by syringe, dried under a gentle stream of argon gas, reconstituted in 36 μL (0.5 mM lipid concentration) of filter-sterilized Dulbecco's phosphate-buffered saline (PBS; D8662, Millipore Sigma), and shaken for 30 min at room temperature (120 RPM). Using a flow cell prepared as described in [Section 2.2](#), 30 μL of prepared lipids were pipetted into the assembled flow cell, sealed (ST200 Adhesive Seal Tabs, Grace Bio-Labs), and incubated at room temperature for 1 h to allow fusion of a bilayer to the surface of the waveguide ([Ando and Skolnick, 2013](#); [Attwood et al., 2013](#)).

2.4 Waveguide assay preparation and blocking

We performed our waveguide assays largely using previously published procedures ([Courtney et al., 2021b](#)). Flow rates were approximately 30 μL/s and incubations occurred at room temperature unless otherwise specified. Using the biosensor described in [Section 2.1](#) and a waveguide with a supported lipid bilayer prepared as described in [Section 2.3](#), the flow cell was washed with 500 μL of PBS and 500 μL of 0.5% bovine serum albumin (BSA; A7906, Millipore Sigma) in PBS. The sensor was aligned by maximizing the intensity of the streak resulting from total internal reflection in the thin film of the waveguide. The lipid bilayer on the waveguide was blocked for 1 h with 500 μL of 2% BSA in PBS and washed with 500 μL of 0.5% BSA in PBS. Five background spectra were recorded.

2.5 Spectral acquisition and processing

All spectra were acquired in a dark room at room temperature with a black box placed on top of the sensor. Spectra had an integration time of 3 s and were recorded from

400–700 nm. Spectra were processed with a ± 3 unweighted moving window average. Background correction was performed by subtracting the most recently acquired background spectrum from the acquired fluorescence spectrum of interest.

2.6 Streptavidin validation assay

We performed our streptavidin validation assay using a waveguide prepared as described in [Section 2.4](#). 200 μL of 100 zM streptavidin-Alexa Fluor 532 conjugate (SA-AF532; S11224, Thermo Fisher Scientific, Waltham, MA, United States) in PBS was prepared by a series of 1:10 dilutions from a 10 nM stock of SA-AF532 in PBS, with mixing by swirling the pipet tip in the tube and pipetting up and down five times between each dilution. The waveguide was incubated for 5 min with the 100 zM SA-AF532 solution (flowed at approximately 20 μL/s) and washed with 500 μL of 0.5% BSA in PBS. Three technical replicate fluorescence spectra were acquired and processed as described in [Section 2.5](#).

2.7 Sandwich immunoassay modelling

Based on the method described by [Zhang et al. \(2014\)](#) we used a Langmuir adsorption model to predict the limit of detection of our modified biosensor in a sandwich immunofluorescence assay ([Langmuir, 2002](#)). We use this model to describe each partitioning exchange in a theoretical surface-based assay:

$$\theta = \theta_{sat} \left(\frac{cK_a}{1 + cK_a} \right) \quad (1)$$

where θ is the number of molecules of analyte adsorbed, θ_{sat} is the saturating (maximum) number of molecules of analyte that can adsorb, c is the concentration of the adsorbing species, and K_a is the association constant describing the binding interaction between the adsorbing species and the surface or receptor to which it adsorbs.

2.8 FEVER probe and influenza oligonucleotide design

The design of the FEVER probe, IAD oligonucleotide, influenza B DNA (IBD) oligonucleotide, and IAR oligonucleotide used in this work (Integrated DNA Technologies, Coralville, IA, United States) has been described previously ([Courtney et al., 2021b](#); [Stromberg et al., 2022](#)). In brief, the FEVER probe is an MB

containing a six-base pair stem sequence (5'-CGCGAT-3'), a 5' 6-carboxyfluorescein (56-FAM) moiety, a 3' black hole quencher-1™ (3BHQ-1) moiety, a biotinylated thymidine residue (BiotT) toward the 3' end, and a 28-base recognition sequence for IAD (3'-/3BHQ-1/**GCG C/BiotT/A TGT TGG TCC CTA GTA ATT AGT CCG TGA GGA GTA GCG C/56-FAM/-5'**; bolded residues denote the stem regions of the probe). The IAD oligonucleotide contains the complement of the 28-base recognition sequence found in the probe (5'-TAA GCA AAA CCC **AGG GAT CAT TAA TCA GGC ACT CCT CAA TTG C-3'**; bolded residues denote the recognition sequence region). Acting as a negative control in these experiments, the IBD oligonucleotide shares at most a sequence of eight consecutive bases with the IAD oligonucleotide, five of which are in the recognition region (5'-TTT GGA CCA TCC ATG CTA TGG TTC TTG GCA TTC **CCT CAA TTA C-3'**; bolded residues denote the sequence shared with the IAD oligonucleotide). The IAR oligonucleotide sequence is the RNA equivalent of the IAD oligonucleotide (5'- UAA GCA AAA CCC **AGG GAU CAU UAA UCA GGC ACU CCU CAA UUG C-3'**; bolded residues denote the recognition sequence region).

2.9 Nucleic acid biosensing preparation

We prepared for our nucleic acid biosensing assays using waveguides prepared as described in Section 2.4. 50 μL of 1 nM SA-AF532 in PBS was incubated on the flow cell for 5 min at room temperature (approximately 20 $\mu\text{L/s}$) and washed with 500 μL of 0.5% BSA in PBS. A fluorescence spectrum of SA-AF532 was recorded to confirm that a lipid bilayer had formed on the surface of the waveguide, and the SA-AF532 on the waveguide was photobleached for 1 h by exposure to the 532-nm laser. 200 μL of unlabeled streptavidin was incubated for 5 min on the surface of the waveguide (approximately 20 $\mu\text{L/s}$) and washed with 500 μL of 0.5% BSA in PBS. A new background spectrum was recorded following photobleaching to use for background subtraction of subsequent spectra.

2.10 Influenza DNA biosensing assays

We used waveguides that were prepared and blocked as described in Section 2.9 for our influenza DNA biosensing assays. Fresh dilutions of influenza DNA and MB were prepared each day by serially diluting (1:100 or 1:10) from 1 nM stocks of IAD and IBD and a 1 μM stock of MB. Each dilution was swirled and pipetted up and down five times to mix.

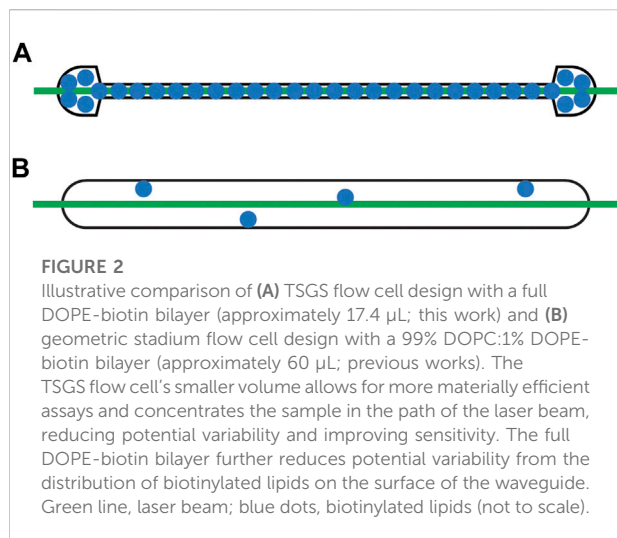
200 μL of MB at 100 zM (an estimated 12 copies of MB) was flowed across the waveguide (approximately 20 $\mu\text{L/s}$) and incubated for 5 min. The flow cell was washed with 500 μL of 0.5% BSA in PBS, the biosensor was briefly aligned (<1 min to

avoid photobleaching) to maximize fluorescent intensity, and the native background fluorescence of the MB was recorded. For the IAD assays, 200 μL of the IAD oligonucleotide at 10 zM in PBS (2 ymol, or $2 \cdot 10^{-24}$ mol, of IAD; an estimated single copy) was flowed across the waveguide (approximately 20 $\mu\text{L/s}$) and incubated for 10 min; for the IBD control assays, 200 μL of the IBD oligonucleotide at 10 aM in PBS (an estimated 1,200 copies of IBD) was flowed across the waveguide (approximately 20 $\mu\text{L/s}$) and incubated for 10 min. Following influenza DNA incubation, the flow cell was washed with 500 μL of 0.5% BSA in PBS, the biosensor was briefly aligned to maximize fluorescent intensity, and the fluorescent signal was recorded as described in Section 2.5. Background-corrected spectra were normalized by division to the peak relative fluorescent intensity of the MB alone. The IAD biosensing assays were performed four times on four separate days by two independent researchers, and the IBD biosensing assays were performed three times on three separate days by two independent researchers.

2.11 Synthetic influenza RNA saliva biosensing assays

We used waveguides that were prepared and blocked as described in Section 2.9 for our influenza RNA biosensing assays in saliva. Fresh dilutions of IAR and MB were prepared each day, serially diluting in PBS (1:5 or 1:10) from a 500 nM stock of IAR and a 1 μM stock of MB with each dilution swirled and pipetted up and down five times to mix. The final 1:10 dilution was performed into a mixture containing 178 μL of normal human saliva (991-05-P, Lee Biosolutions, Maryland Heights, MO, United States) and 2 μL RNase inhibitor (AM2696, Thermo Fisher Scientific), yielding a final concentration of 1% RNase inhibitor by volume in a final volume of 200 μL .

200 μL of MB at 100 zM in PBS was flowed across the waveguide (approximately 20 $\mu\text{L/s}$) and incubated for 5 min. The flow cell was washed with 500 μL of 0.5% BSA in PBS, the biosensor was briefly aligned to maximize fluorescent signal, and the native background fluorescence of the MB was recorded. 200 μL of normal human saliva containing 1% RNase inhibitor by volume was flowed across the waveguide (approximately 20 $\mu\text{L/s}$) and incubated for 10 min; the flow cell was washed with 500 μL of 0.5% BSA in PBS, the biosensor was briefly aligned to maximize fluorescent intensity, and the nonspecific background fluorescence from saliva was recorded. 200 μL of the IAR oligonucleotide at 10 zM (2 ymol of IAR; an estimated single copy) spiked into normal human saliva containing 1% RNase inhibitor by volume was flowed across the waveguide (approximately 20 $\mu\text{L/s}$) and incubated for 10 min; the flow cell was washed with 500 μL of 0.5% BSA in PBS, the biosensor was briefly aligned to maximize fluorescent intensity, and the specific fluorescence from 10 zM IAR in saliva was recorded as described



in Section 2.5. 200 μL of IAR oligonucleotide at 50 zM, 100 zM, and 1 aM (an estimated six, 12, and 120 copies of IAR, respectively) in saliva with 1% RNase inhibitor by volume were subsequently tested on the same waveguide in the same manner. Background-corrected spectra were normalized by division to the peak relative fluorescent intensity of the MB alone. The IAR biosensing assays were performed three times on three separate days by three independent researchers.

2.12 Genomic influenza RNA saliva biosensing assays

Genomic RNA isolated from influenza A virus, A/Hong Kong/8/1968 (H3N2) (catalog no. NR-2774) was obtained from BEI Resources (Manassas, VA, United States). The sample was serially diluted in PBS and finally in saliva by the same assay protocol performed above except injections of genomic IAR were 100 μL at approximately 50,000 genome equivalents ($5 \cdot 10^4$ genome copies/mL).

3 Results and discussion

3.1 Methods comparison

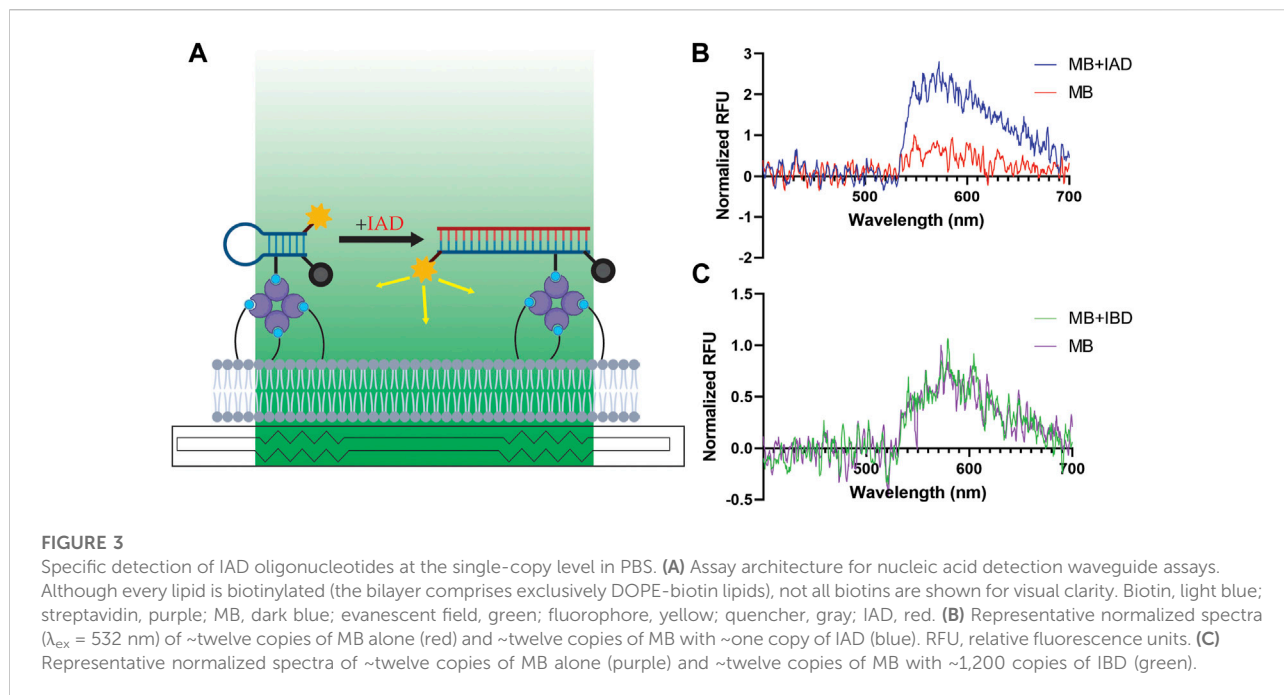
A comparison between the new methods described here (flow cell geometry and bilayer composition) and our previous methods is shown in Figure 2. Our TSGS flow cell design (Figure 2A) has multiple benefits over our previous flow cell design (Figure 2B). The TSGS cell's smaller volume (approximately 17.4 μL , as compared to approximately 60 μL for the previous flow cell design) allows us to reduce the amount of buffer per wash and sample per incubation without changing

the concentration, yielding a more materially efficient assay (Kocheril et al., 2022). The TSGS flow cell was made smaller by reducing the width across the middle of the flow cell; this change theoretically 1) reduces sampling variability in experiments by irradiating almost the entire flow cell and 2) allows for the sensor to measure samples at lower concentration because analytes are effectively concentrated in the path of the laser. Additionally, a bilayer consisting exclusively of DOPE-biotin, instead of the 99% dioleoyl phosphocholine (DOPC): 1% DOPE-biotin bilayers that were previously used, further reduces potential variability from lipid distribution on the surface of the waveguide and provides a fully biotinylated surface, effectively allowing for complete capture of streptavidin ($K_a = 2.5 \cdot 10^{13} \text{ M}^{-1}$) (Mukundan et al., 2012; Deng et al., 2013). Furthermore, in this work we have demonstrated the viability of a 1-h incubation at room temperature to allow fusion of a lipid bilayer to the waveguide surface instead of the 16-h overnight incubation that we previously performed, allowing our assays to be completed in a single day instead of two.

Using these new experimental procedures, we assessed the instrumental sensitivity of our modified biosensor with highly dilute SA-AF532 and confirmed that our biosensor is able to measure fluorescence from fluorescent analytes at the single-molecule level (see Supplementary Material S1; Supplementary Figure S1). Additionally, we explored the applicability of our biosensor in a theoretical sandwich immunoassay format using a Langmuir adsorption model (see Supplementary Material S1; Supplementary Figure S2). Notably, this model does not account for nonspecific interactions, which are a significant challenge in sandwich immunoassays (Mukundan et al., 2012). Furthermore, the sensitivity and specificity of Abs are known to vary significantly (Smith et al., 1970; Stanley et al., 1983; Friguier et al., 1985; Karlsson et al., 1991; Malmqvist, 1993; Janeway et al., 2001; Heinrich et al., 2010; Zhang et al., 2014; Landry et al., 2015). Therefore, we expect that Ab-based assays performed with this biosensor in future work will be limited only by the specificity, sensitivity, and quantity of the Abs used in the assay (see Supplementary Material S1 for more information).

3.2 Influenza DNA biosensing assays

To assess our new sensing capabilities in a biologically relevant assay architecture, we performed sensing assays with highly dilute MBs and IAD oligonucleotides, using IBD oligonucleotides as a negative control to assess the specificity of our MBs. Our DNA assay architecture is shown in Figure 3A, and representative fluorescence spectra with IAD and IBD are shown in Figures 3B,C respectively. As shown in Figures 3B,C, the MB alone does exhibit some native fluorescence, suggesting that the MB retains some degree of conformational freedom and can open from its quenched stem-loop structure to a fluorescent



straight-chain structure even in the absence of a hybridizing complementary nucleic acid, if only transiently. We observed similar nonspecific fluorescence in our previous report describing detection of viral RNAs, citing the magnitude of the nonspecific signal as a limiting factor in the sensitivity of our biosensor (Courtney et al., 2021b). However, the nonspecific fluorescence observed in this work was drastically reduced because we 1) used much smaller quantities of MB here (previous: 100 μL at 100 nM—an estimated six trillion copies of MB; this work: 200 μL at 100 zM—an estimated twelve copies of MB), thereby reducing the total background fluorescence, and 2) used an MB tagged with fluorescein (this work) instead of Alexa Fluor 532 (previous). Alexa Fluor 532 is a bright, high-efficiency fluorophore ($\lambda_{\text{ex}} = 530$, $\lambda_{\text{em}} = 553 \text{ nm}$) that is easily excited by 532-nm laser light (99% excitation efficiency; Fluorescence SpectraViewer, Thermo Fisher Scientific), making complete quenching difficult. In contrast, because fluorescein's excitation maximum is 495 nm, its excitation efficiency is significantly hindered when excited with 532-nm laser light (3% excitation efficiency; Fluorescence SpectraViewer, Thermo Fisher Scientific), meaning that the quencher attached to the MB is better able to quench the fluorophore when the MB is in a stem-loop conformation. Although fluorescein does have some intrinsic disadvantages, such as deviation from ideal Stern–Volmer behavior at high concentrations, the highly dilute concentrations used here likely avoid aggregation-related issues (Aldrich et al., 2021). We attribute the significant enhancement in sensitivity presented in this work to these factors, in addition to the benefits of the TSGS flow cell and full DOPE-biotin bilayer described in Section 3.1.

The significant increase in fluorescent intensity following addition of IAD (Figure 3B) suggests that the estimated single copy of IAD has hybridized with an MB held to the surface of the waveguide. The sensitivity of this method comes from a variety of factors, including 1) the strong hybridization affinity between complementary nucleic acids, 2) the separation of solution contaminants and surface-bound analytes, 3) the high-quantum yield fluorophore used on the molecular beacon, and 4) the integration of fluorescent emission (a process that occurs on the order of nanoseconds) over a total of 3 seconds. We observed similar increases in three of our four trials with IAD in total. As noted in the introduction, sampling variability is a significant challenge in experimentation at the single-molecule level. In the experiment that did not yield a significant increase in fluorescent emission upon addition of IAD, the background signal from the MB was essentially zero, suggesting that there may have been no MBs on the surface of the waveguide in that particular assay (likely due to the MBs sticking to the walls of the syringe used to inject the MB solution into the flow cell, the tip of the micropipette used to prepare the solution, and/or the tube in which the solution was prepared).

The absence of a significant increase in fluorescent intensity following addition of IBD (Figure 3C) indicates that the increase in fluorescence observed upon addition of IAD (Figure 3B) depends on the sequence of the added oligonucleotide, lending confidence to the specificity of the assay. Notably, an estimated 1,200 copies of IBD were used in these control experiments, and no enhancement of fluorescent intensity was observed in any of the three replicate IBD experiments. Therefore, our control experiments with IBD suggest that our

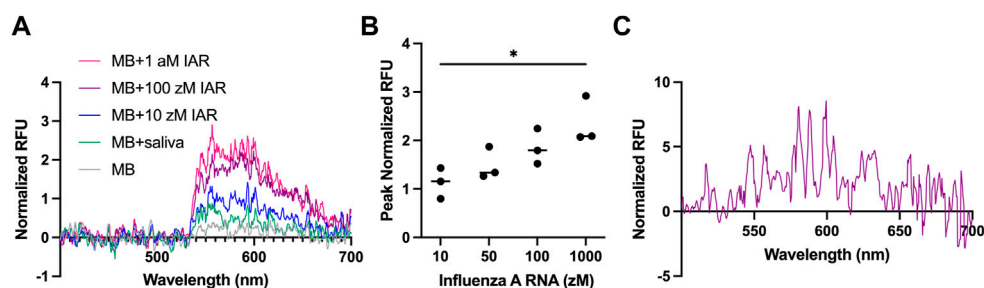


FIGURE 4

Detection of IAR in saliva. (A) Representative normalized spectra ($\lambda_{\text{ex}} = 532 \text{ nm}$) of synthetic IAR oligonucleotides in 200 μL of saliva (10 zM, blue; 100 zM; purple; 1 a.m., pink) compared to saliva alone (green) and the molecular beacon (MB) in buffer alone (gray). 10 zM represents estimated single-copy level. All saliva samples contained 1% RNase inhibitor by volume. RFU, relative fluorescence units. (B) Peak normalized fluorescent intensity as a function of synthetic IAR concentration in saliva. Error bars are \pm one standard deviation. A one-way ANOVA followed by Tukey's method for multiple means comparison was used to compare the sensor responses at the various concentrations studied ($*p < 0.033$). Analyses were performed using Prism (v9, GraphPad Software, San Diego, CA, United States). (C) Detection of 4.69 \log_{10} copies/mL of genomic IAR presented as normalized spectra ($\lambda_{\text{ex}} = 532 \text{ nm}$).

MB is selective and exhibits a robust resistance to even a saturating excess of a non-targeted oligonucleotide. For further information on the selectivity of MBs from the FEVER computational pipeline, see [Stromberg et al., 2022](#) and [Courtney et al., 2021b](#).

3.3 Influenza RNA biosensing assays

To assess the performance of our modified biosensor in a physiologically meaningful context, we performed biosensing assays with highly dilute IAR spiked into normal human saliva and used blank saliva from the same stock as a negative control. As shown in [Figure 4A](#), the presence of control saliva leads to a small increase in the nonspecific background fluorescence of the MB. The addition of an estimated single copy of synthetic IAR oligonucleotide (200 μL at 10 zM in saliva) results in a noticeable increase in observed fluorescent intensity, suggesting specific detection of IAR at the single-copy level in a complex biofluid sample with our fluorescence-based waveguide biosensor. Upon addition of 200 μL of 100 zM IAR in saliva (an estimated twelve copies of IAR; 1:1 with the estimated amount of MB on the surface of the waveguide), we see a substantial increase in fluorescent intensity over the saliva background, and at a tenfold excess of IAR (200 μL of 1 aM IAR in saliva), we appear to see saturation of the MB ([Figure 4B](#)). This concentration-dependent increase in fluorescent intensity was consistent over three experiments performed on three separate days by two independent researchers, lending confidence to the reproducibility of our data (coefficient of variation average 22.65%; [Supplementary Table S1](#)). Fitting of the data to a sigmoid curve produced an r^2 of 0.6817, further suggesting saturation of the MB (see [Supplementary Material S1](#); [Supplementary Figure S3](#)). Compared to the lowest

concentration at which we previously demonstrated detection of IAR in saliva (100 μL at 100 nM—an estimated six trillion copies), this work constitutes a sensitivity enhancement of over a trillion-fold. To demonstrate the feasibility of detecting an actual viral sample in saliva, we assayed genomic IAR isolated from influenza A virus A/Hong Kong/8/1968 ([Figure 4C](#)) that was spiked into normal human saliva. As expected, the signal is noisier when detecting genomic RNA as compared with the exact-match synthetic IAR oligonucleotides used in [Figure 4A](#). However, a clear increase in background-corrected signal intensity is observed with genomic IAR at 4.69 \log_{10} viral copies/mL ($5 \cdot 10^4$ copies/mL), which is a clinically relevant concentration for upper respiratory viruses in saliva ([To et al., 2017](#); [Carrouel et al., 2022](#)).

4 Conclusion

Using a TSGS flow cell and a fully biotinylated lipid bilayer, we have performed fluorimetry assays with MBs that indicate specific detection of IAD oligonucleotides in PBS and IAR oligonucleotides spiked into normal human saliva in yoctomole quantities (200 μL at 10 zM—an estimated single copy). We also detected isolated genomic influenza A RNA spiked into saliva at clinically relevant concentrations. These assays were performed entirely without nucleic acid amplification. Although our total assay time was roughly 4 hours, it could be reduced to approximately two and a half hours by removing the SA-AF532 incubation and photobleaching steps. Furthermore, the assay time following addition of the saliva sample was under 15 minutes. Waveguide-based biosensing using MBs holds significant potential as a means of achieving rapid, specific, accessible, and amplification-free nucleic acid diagnostics.

Out of an abundance of caution, we again emphasize that sampling variability is a significant challenge in experiments at the single-molecule level, and we note that our sample sizes are small. We cannot entirely rule out the possibilities that MB diffusion in the bilayer over time, slight differences in optical alignment, non-uniform fluid distributions, molecules sticking to the walls of tubes or pipet tips, or other factors may skew the results of the spectra presented in this manuscript. Although the results of our control experiments with IBD and blank saliva suggest that our biosensor is capable of measuring specific signals from nucleic acid targets at or near the single-copy level, we maintain that the results presented here should be viewed as preliminary and illustrative of the sensitivity improvements that are possible with optimized experimental design.

Data availability statement

The datasets presented in this study can be found in online repositories. The names of the repository/repositories and accession numbers can be found below: The datasets generated for this study can be found on Figshare (<https://doi.org/10.6084/m9.figshare.19449989>).

Author contributions

PK: Conceptualization, methodology, software, validation, formal analysis, investigation, data curation, writing—original draft preparation, writing—review and editing, visualization. KL: Conceptualization, validation, formal analysis, investigation, data curation, writing—review and editing, supervision. DJ: Conceptualization, methodology, validation, formal analysis, investigation, writing—review and editing. JK-S: Conceptualization, validation, formal analysis, investigation, resources, writing—review and editing, supervision, project administration, funding acquisition.

Funding

This work was funded by the Laboratory Directed Research and Development program of Los Alamos National Laboratory (Grant Number 20190392 ER) as well as a Strategic Investment

References

Akkilic, N., Geschwindner, S., and Hook, F. (2020). Single-molecule biosensors: Recent advances and applications. *Biosens. Bioelectron.* *X*, 151, 111944. doi:10.1016/j.bios.2019.111944

Aldrich, K. E., Livshits, M. Y., Stromberg, L. R., Janicke, M. T., Nhu Lam, M., Stein, B., et al. (2021). Th(IV)-Desferrioxamine: Characterization of a fluorescent bacterial probe. *Dalton Trans.* 50, 15310–15320. doi:10.1039/d1dt02177j

Initiative of the Richard P. Feynman Center for Innovation. The funders had no role in the study design; the collection, analysis, and interpretation of data; the writing of the report; and the decision to submit the article for publication.

Acknowledgments

PK thanks Marissa Weichman for the inspiration to pursue single-molecule detection. Figure 3A, Supplementary Figures S1A, S2 were created with BioRender.com. The following reagent was obtained through BEI Resources, NIAID, NIH: Genomic RNA from Influenza A Virus, A/Hong Kong/8/1968 (H3N2), NR-2774. This work was performed at the Los Alamos National Laboratory, which is operated by Triad National Security, LLC, for the National Nuclear Security Administration of the U.S. Department of Energy (contract number 89233218CNA000001). The views expressed in this article are those of the authors and do not reflect the official policy or position of the U.S. Government.

Conflict of interest

The authors declare that the research was conducted in the absence of any commercial or financial relationships that could be construed as a potential conflict of interest.

Publisher's note

All claims expressed in this article are solely those of the authors and do not necessarily represent those of their affiliated organizations, or those of the publisher, the editors and the reviewers. Any product that may be evaluated in this article, or claim that may be made by its manufacturer, is not guaranteed or endorsed by the publisher.

Supplementary material

The Supplementary Material for this article can be found online at: <https://www.frontiersin.org/articles/10.3389/fsens.2022.948466/full#supplementary-material>

Aman, R., Mahas, A., and Mahfouz, M. (2020). Nucleic acid detection using CRISPR/cas biosensing technologies. *ACS Synth. Biol.* *9*, 1226–1233. doi:10.1021/acssynbio.9b00507

Ando, T., and Skolnick, J. (2013). On the importance of hydrodynamic interactions in lipid membrane formation. *Biophys. J.* *104*, 96–105. doi:10.1016/j.bpj.2012.11.3829

- Assad, O. N., Gilboa, T., Spitzberg, J., Juhasz, M., Weinhold, E., and Meller, A. (2017). Light-enhancing plasmonic-nanopore biosensor for superior single-molecule detection. *Adv. Mat.* 29, 1605442. doi:10.1002/adma.201605442
- Attwood, S. J., Choi, Y., and Leonenko, Z. (2013). Preparation of DOPC and DPPC supported planar lipid bilayers for atomic Force microscopy and atomic Force spectroscopy. *Int. J. Mol. Sci.* 14, 3514–3539. doi:10.3390/ijms14023514
- Baaske, M. D., Foreman, M. R., and Vollmer, F. (2014). Single-molecule nucleic acid interactions monitored on a label-free microcavity biosensor platform. *Nat. Nanotechnol.* 9, 933–939. doi:10.1038/nnano.2014.180
- Battich, N., Stoeger, T., and Pelkmans, L. (2013). Image-based transcriptomics in thousands of single human cells at single-molecule resolution. *Nat. Methods* 10, 1127–1133. doi:10.1038/nmeth.2657
- Benito-Pena, E., Valdes, M. G., Glahn-Martinez, B., and Moreno-Bondi, M. C. (2016). Fluorescence based fiber optic and planar waveguide biosensors. A review. *Anal. Chim. Acta* X. 943, 17–40. doi:10.1016/j.aca.2016.08.049
- Carrouel, F., Gadea, E., Esparcieux, A., Dimet, J., Langlois, M. E., Perrier, H., et al. (2022). Saliva quantification of SARS-CoV-2 in real-time PCR from asymptomatic or mild COVID-19 adults. *Front. Microbiol.* 12, 786042. doi:10.3389/fmicb.2021.786042
- Chen, C., and Wang, J. (2020). Optical biosensors: An exhaustive and comprehensive review. *Analyst* 145, 1605–1628. doi:10.1039/c9an01998g
- Cohen, L., and Walt, D. R. (2017). Single-molecule arrays for protein and nucleic acid analysis. *Annu. Rev. Anal. Chem. Palo. Alto. Calif.* 10, 345–363. doi:10.1146/annurev-anchem-061516-045340
- Courtney, S. J., Stromberg, Z. R., and Kubicek-Sutherland, J. Z. (2021a). Nucleic acid-based sensing techniques for diagnostics and surveillance of influenza. *Biosensors* 11, 47. doi:10.3390/bios11020047
- Courtney, S. J., Stromberg, Z. R., Myers Y Gutiérrez, A., Jacobsen, D., Stromberg, L. R., Lenz, K. D., et al. (2021b). Optical biosensor platforms display varying sensitivity for the direct detection of influenza RNA. *Biosensors* 11, 367. doi:10.3390/bios11100367
- Deng, L., Kitova, E. N., and Klassen, J. S. (2013). Dissociation kinetics of the streptavidin-biotin interaction measured using direct electrospray ionization mass spectrometry analysis. *J. Am. Soc. Mass Spectrom.* 24, 49–56. doi:10.1007/s13361-012-0533-5
- Du, Y., and Dong, S. (2017). Nucleic acid biosensors: Recent advances and perspectives. *Anal. Chem.* 89, 189–215. doi:10.1021/acs.analchem.6b04190
- Fan, S., Webb, J. E. A., Yang, Y., Nieves, D. J., Goncales, V. R., Tran, J., et al. (2019). Observing the reversible single molecule electrochemistry of Alexa fluor 647 dyes by total internal reflection fluorescence microscopy. *Angew. Chem. Int. Ed. Engl.* 58, 14637–14640. doi:10.1002/ange.201907298
- Fraze, B. W., Rodriguez-Hoces De La Guardia, A., Alter, H., Chen, C. G., Fuentes, E. L., Holzer, A. K., et al. (2018). Accuracy and discomfort of different types of intranasal specimen collection methods for molecular influenza testing in emergency department patients. *Ann. Emerg. Med.* 71, 509–517.e1. doi:10.1016/j.annemergmed.2017.09.010
- Friguet, B., Chaffotte, A. F., Djavadi-Ohanian, L., and Goldberg, M. E. (1985). Measurements of the true affinity constant in solution of antigen-antibody complexes by enzyme-linked immunosorbent assay. *J. Immunol. Methods* 77, 305–319. doi:10.1016/0022-1759(85)90044-4
- Golden, J. P., Taitt, C. R., Shriver-Lake, L. C., Shubin, Y. S., and Ligler, F. S. (2005). A portable automated multianalyte biosensor. *Talanta* 65, 1078–1085. doi:10.1016/j.talanta.2004.03.072
- Grace, K. M., Goeller, R. M., Grace, W. K., Kolar, J. D., Morrison, L. J., Sweet, M. R., et al. (2004). “Reagentless optical biosensor,” in *Chemical and biological point sensors for homeland defense* (Bellingham, Washington, United States: SPIE).
- Heinrich, L., Tissot, N., Hartmann, D. J., and Cohen, R. (2010). Comparison of the results obtained by ELISA and surface plasmon resonance for the determination of antibody affinity. *J. Immunol. Methods* 352, 13–22. doi:10.1016/j.jim.2009.10.002
- Huang, T., Nallathamby, P. D., and Xu, X. H. (2008). Photostable single-molecule nanoparticle optical biosensors for real-time sensing of single cytokine molecules and their binding reactions. *J. Am. Chem. Soc.* 130, 17095–17105. doi:10.1021/ja8068853
- Janeway, C. A., Jr., Travers, P., Walport, M., and Shlomchik, M. (2001). *Immunobiology: The Immune system in Health and disease*. New York, NY, USA: Garland Science.
- Johnson-Buck, A., Su, X., Giraldez, M. D., Zhao, M., Tewari, M., and Walter, N. G. (2015). Kinetic fingerprinting to identify and count single nucleic acids. *Nat. Biotechnol.* 33, 730–732. doi:10.1038/nbt.3246
- Karlsson, R., Michaelsson, A., and Mattsson, L. (1991). Kinetic analysis of monoclonal antibody-antigen interactions with a new biosensor based analytical system. *J. Immunol. Methods* 145, 229–240. doi:10.1016/0022-1759(91)90331-9
- Kelley, S. O. (2017). What are clinically relevant levels of cellular and biomolecular analytes? *ACS Sens.* 2, 193–197. doi:10.1021/acssensors.6b00691
- Kocheril, P. A., Lenz, K. D., Mascareñas, D. D. L., Morales-García, J. E., Anderson, A. S., and Mukundan, H. (2022). Portable waveguide-based optical biosensor. *Biosensors* 12, 195. doi:10.3390/bios12040195
- Kumar, S., and Henrickson, K. J. (2012). Update on influenza diagnostics: Lessons from the novel H1N1 influenza A pandemic. *Clin. Microbiol. Rev.* 25, 344–361. doi:10.1128/cmr.05016-11
- Landry, J. P., Ke, Y., Yu, G. L., and Zhu, X. D. (2015). Measuring affinity constants of 1450 monoclonal antibodies to peptide targets with a microarray-based label-free assay platform. *J. Immunol. Methods* 417, 86–96. doi:10.1016/j.jim.2014.12.011
- Landry, M. P., Ando, H., Chen, A. Y., Cao, J., Kottadiel, V. I., Chio, L., et al. (2017). Single-molecule detection of protein efflux from microorganisms using fluorescent single-walled carbon nanotube sensor arrays. *Nat. Nanotechnol.* 12, 368–377. doi:10.1038/nnano.2016.284
- Langmuir, I. (2002). The adsorption of gases on plane surfaces of glass, mica and platinum. *J. Am. Chem. Soc.* 40, 1361–1403. doi:10.1021/ja02242a004
- Lee, N., Chan, P. K., Hui, D. S., Rainer, T. H., Wong, E., Choi, K. W., et al. (2009). Viral loads and duration of viral shedding in adult patients hospitalized with influenza. *J. Infect. Dis.* 200, 492–500. doi:10.1086/600383
- Li, Y., Yang, C., and Guo, X. (2020). Single-molecule electrical detection: A promising route toward the fundamental limits of chemistry and life science. *Acc. Chem. Res.* 53, 159–169. doi:10.1021/acs.accounts.9b00347
- Liu, L., Zhou, X., Lu, M., Zhang, M., Yang, C., Ma, R., et al. (2017a). An array fluorescent biosensor based on planar waveguide for multi-analyte determination in water samples. *Sensors Actuators B Chem.* 240, 107–113. doi:10.1016/j.snb.2016.08.118
- Liu, L., Zhou, X., Wilkinson, J. S., Hua, P., Song, B., and Shi, H. (2017b). Integrated optical waveguide-based fluorescent immunosensor for fast and sensitive detection of microcystin-LR in lakes: Optimization and Analysis. *Sci. Rep.* 7, 3655. doi:10.1038/s41598-017-03939-8
- Long, G. L., and Winefordner, J. D. (1983). Limit of detection. A closer look at the IUPAC definition. *Anal. Chem.* 55, 712A–724A. doi:10.1021/ac00258a724
- Ma, F., Li, C. C., and Zhang, C. Y. (2021). Nucleic acid amplification-integrated single-molecule fluorescence imaging for *in vitro* and *in vivo* biosensing. *Chem. Commun.* 57, 13415–13428. doi:10.1039/d1cc04799j
- Malmqvist, M. (1993). Surface plasmon resonance for detection and measurement of antibody-antigen affinity and kinetics. *Curr. Opin. Immunol.* 5, 282–286. doi:10.1016/0952-7915(93)90019-o
- Mauranyapin, N. P., Madsen, L. S., Taylor, M. A., Waleed, M., and Bowen, W. P. (2017). Evanescent single-molecule biosensing with quantum-limited precision. *Nat. Photonics* 11, 477–481. doi:10.1038/nphoton.2017.99
- Moerner, W. E., and Fromm, D. P. (2003). Methods of single-molecule fluorescence spectroscopy and microscopy. *Rev. Sci. Instrum.* 74, 3597–3619. doi:10.1063/1.1589587
- Moerner, W. E., and Kador, L. (1989). Optical detection and spectroscopy of single molecules in a solid. *Phys. Rev. Lett.* 62, 2535–2538. doi:10.1103/physrevlett.62.2535
- Mukundan, H., Anderson, A. S., Grace, W. K., Grace, K. M., Hartman, N., Martinez, J. S., et al. (2009). Waveguide-based biosensors for pathogen detection. *Sensors* 9, 5783–5809. doi:10.3390/s90705783
- Mukundan, H., Kumar, S., Price, D. N., Ray, S. M., Lee, Y. J., Min, S., et al. (2012). Rapid detection of *Mycobacterium tuberculosis* biomarkers in a sandwich immunoassay format using a waveguide-based optical biosensor. *Tuberculosis* 92, 407–416. doi:10.1016/j.tube.2012.05.009
- Nakane, J., Wiggan, M., and Marzali, A. (2004). A nanosensor for transmembrane capture and identification of single nucleic acid molecules. *Biophys. J.* 87, 615–621. doi:10.1529/biophysj.104.040212
- Orrit, M., and Bernard, J. (1990). Single pentacene molecules detected by fluorescence excitation in a p-terphenyl crystal. *Phys. Rev. Lett.* 65, 2716–2719. doi:10.1103/physrevlett.65.2716
- Smith, T. W., Butler, V. P., Jr., and Haber, E. (1970). Characterization of antibodies of high affinity and specificity for the digitalis glycoside digoxin. *Biochemistry* 9, 331–337. doi:10.1021/bi00804a020
- Sohn, S., and Kim, D. (2005). Modification of Langmuir isotherm in solution systems-definition and utilization of concentration dependent factor. *Chemosphere* 58, 115–123. doi:10.1016/j.chemosphere.2004.08.091
- Stanley, C., Lew, A. M., and Steward, M. W. (1983). The measurement of antibody affinity: A comparison of five techniques utilizing a panel of monoclonal anti-DNP antibodies and the effect of high affinity antibody

on the measurement of low affinity antibody. *J. Immunol. Methods* 64, 119–132. doi:10.1016/0022-1759(83)90390-3

Stromberg, Z. R., Theiler, J., Foley, B. T., Myers Y Gutiérrez, A., Hollander, A., Courtney, S. J., et al. (2022). Fast evaluation of viral emerging risks (FEVER): A computational tool for biosurveillance, diagnostics, and mutation typing of emerging viral pathogens. *PLOS Glob. Public Health* 2, e0000207. doi:10.1371/journal.pgph.0000207

Taitt, C. R., Anderson, G. P., and Ligler, F. S. (2016). Evanescent wave fluorescence biosensors: Advances of the last decade. *Biosens. Bioelectron.* X, 76, 103–112. doi:10.1016/j.bios.2015.07.040

To, K. K., Lu, L., Yip, C. C., Poon, R. W., Fung, A. M., Cheng, A., et al. (2017). Additional molecular testing of saliva specimens improves the detection of respiratory viruses. *Emerg. Microbes Infect.* 6, 1–7. doi:10.1038/emi.2017.35

To, K. K. W., Yip, C. C. Y., Lai, C. Y. W., Wong, C. K. H., Ho, D. T. Y., Pang, P. K. P., et al. (2019). Saliva as a diagnostic specimen for testing respiratory virus by a point-of-care molecular assay: A diagnostic validity study. *Clin. Microbiol. Infect.* 25, 372–378. doi:10.1016/j.cmi.2018.06.009

Wong, C. H., Nguyen, L., Peh, J., Luu, L. M., Sanchez, J. S., Richardson, S. L., et al. (2014). Targeting toxic RNAs that cause myotonic dystrophy type 1 (DM1) with a bisamidinium inhibitor. *J. Am. Chem. Soc.* 136, 6355–6361. doi:10.1021/ja5012146

Zevenbergen, M. A., Singh, P. S., Goluch, E. D., Wolfrum, B. L., and Lemay, S. G. (2011). Stochastic sensing of single molecules in a nanofluidic electrochemical device. *Nano Lett.* 11, 2881–2886. doi:10.1021/nl2013423

Zhang, S., Garcia-D'angeli, A., Brennan, J. P., and Huo, Q. (2014). Predicting detection limits of enzyme-linked immunosorbent assay (ELISA) and bioanalytical techniques in general. *Analyst* 139, 439–445. doi:10.1039/c3an01835k